Bromozincate ionic liquids in the Knoevenagel condensation reaction

Lisa C. Player, Bun Chan, Peter Turner, Anthony F. Masters, Thomas Maschmeyer*

Laboratory of Advanced Catalysis for Sustainability, School of Chemistry, The University of Sydney, Sydney 2006, Australia

A R T I C L E   I N F O

A B S T R A C T

Ionic liquids (ILs) have been widely promoted as functional replacements of volatile organic solvents; however restricting their use to conventional solvents constrains their potential. One means of enhancing their utility is through the development of dual purpose ILs, capable of acting as both solvent and catalyst. A series of bromozincate ILs was synthesised, and the Lewis acidities probed spectroscopically. Furthermore, the crystal and molecular structure of $[C_2Py]_2[ZnBr_4]$ was determined through single-crystal X-ray diffraction. The ILs were then used in a model reaction, aimed at probing effects of both IL Lewis acidity and structural organisation on the reaction outcome.

1. Introduction

Currently, most non-aqueous solvents used in industrial applications are major contributors to industrial waste and pose detrimental effects to both human health and the environment. Ionic liquids (ILs) have received widespread attention as an environmentally benign alternative to organic solvents in a variety of reaction systems, due to their recyclability, low vapour pressure and low flammability resulting in a reduction in hazards associated with solvent use. Moreover, the large number of potential anion and cation combinations allows for an extensive variety in tailorable functionalities [1–5].

In addition to directly influencing the solvation environment, ILs have been shown to exhibit distinctive internal structural features, such as the formation of heterogeneous structures, i.e. with the segregation of polar and non-polar domains [6,7]. This domain segregation, referred to as nano-segregation is one of the features that distinguishes ILs from the homogeneous environment of organic solvents, and offers an approach to control the characteristics of a reaction (rate, selectivity etc.) through IL modification. As demonstrated by both simulation [8,9] and experiment [10], polar solutes will preferentially solvate in the polar domain and non-polar solutes in the non-polar domains of ILs, permitting the encapsulation or partitioning of solutes in specific domains. This phenomenon has been shown to significantly affect chemical reactivity [10], it is frequently overlooked.

An extension of the use of ILs as solvents, is the development of dual purpose ILs, such that a single IL may act as both catalyst and solvent [11]. Several Lewis acidic ILs have been used previously as dual purpose solvents and catalysts, the most common the chloroaluminate anion [12,13]. However issues with handling and synthesis limit the

practical use of this class of material. The work reported here outlines the use of bromozincate ILs [14] which overcome handling barriers and offers an affordable and more environmentally benign alternative to more corrosive and reactive materials. We also report the influence of Lewis acidity and internal organization of these ILs on a model reaction. The cations used and the corresponding abbreviations employed throughout this work are depicted in Fig. 1.

2. Experimental

2.1. Chemical reagents

The following reagents were used as received: benzaldehyde, pyridine (both Ajax), anhydrous zinc bromide, 1-bromobutane, 1-bromohexane, 1-bromodecane, 1,2-dimethylimidazole, 1-methylimidazole (Aldrich), malononitrile (Alfa), *p*-isopropyltoluene (> 99%; Fluka), 1-bromoethane, 1-bromooctane (both Merck). Diethyl ether, hexane and dichloromethane (DCM) were deoxygenated and dried over activated alumina, using an apparatus modified from that described in the literature [15].

2.2. Ionic liquid synthesis

Bromide containing ILs were synthesised using standard literature methods [16]. The syntheses of bromozincate containing ILs were based on a synthetic approach from Abbott et al. [17]. The desired bromide salt (8.9 mmol) was mixed with anhydrous zinc bromide ($ZnBr_2$, 8.9 mmol), and heated to 60 °C under nitrogen. The resulting compound was then cooled and washed with diethyl ether (2 × 10 mL),

---

Fig. 1. Schematic illustrations and nomenclature of cations used in this work, where R = $(CH_2)_{n-1}CH_3$, n = *2, 4, 6, 8, 10.*

and hexane (10 mL) and dried under vacuum, yielding the desired bromozincate IL. A list of ILs prepared in this work and their full physical characterisation data including ^{1}H NMR, ^{13}C NMR, DSC, TGA and ± ESI/MS are available in the ESI. Water content of the ILs was determined using a Karl Fischer coulombic titrator (Mettler Toledo) and was found to be ≤10 ppm.

2.3. Ionic liquid characterisation

2.3.1. X-ray crystallography

Colourless blade-like crystals of $[C_2Py]Br/ZnBr_2$ were grown on standing the IL in methanol for 24 h. The crystal structure was solved in the monoclinic space group $C_{2/c}$ by direct methods with SHELXT [18] and extended and refined with SHELXL-2014/7 [19], with the formula resolved to be $[C_2Py]_2[ZnBr_4]$. Refer to ESI for further details.

2.3.2. Computational predictions through density functional theory

Density functional theory (DFT) quantum chemical calculations were performed with Gaussian 09 [20]. Geometries and energy densities were obtained at the M05-2X/6-31G(d) level, combined with the SMD continuum solvation model [21,22]. Acetonitrile solvation parameters were used in the SMD model. Vibration frequencies of stationary points corresponded to the minima on the potential energy surface. Incorporated into the total energies are zero-point vibrational energies and thermal corrections for enthalpy and entropy derived from scaled M05-2X-D3/6- 31G(d) frequencies [23]. All free energies (kJ mol^{-1}) are reported as solvation-corrected at 298 K, and charges on zinc were calculated using natural bond orbital (NBO) analysis.

2.3.3. Raman spectroscopy

Raman spectra were recorded on a Renishaw Raman Reflex inVia spectrometer fitted with a Leica DMLM microscope. A 514 nm laser was used over the range: 100–2000 cm^{-1}, with a resolution of 4 cm^{-1}. Absorption maximum values were obtained by direct peak picking from raw spectra.

2.3.4. Lewis acidity determination of bromozincate ILs

The Lewis acidity of the ILs was spectroscopically probed with pyridine in a similar method to that previously reported by Yang et al. [24]. Samples were prepared with a mass ratio of pyridine to IL (1:3). FT-IR spectra were obtained using a thin film method with sodium chloride cells on a Bruker Vertex 80V FTIR Spectrometer over the range 1600 and 1400 cm^{-1} at room temperature, with a resolution of 0.2 cm^{-1}. Three repeat scans were performed and the spectra averaged.

2.4. Knoevenagel condensation reactions

2.4.1. Synthesis of 2-benzylidenemalononitrile

For calibration 2-benzylidenemalononitrile was synthesised as follows: Benzaldehyde (2 g, 19 mmol) was mixed with malononitrile (1.25 g, 19 mmol) and heated at 80 °C for 4 h. The yellow crystals formed were washed with water, and recrystallized from methanol, to yield fine white crystals of 2-benzylidenemalononitrile (2.23 g, 24 mmol, 65%, m.p. 82–85 °C). ^{1}H NMR (CDCl$_3$, ppm) δ 7.90 (m, 2H), 7.61 (m, 1H), 7.78 (s, 1H), 7.54 (m, 2H). ^{13}C{^{1}H} NMR (CDCl$_3$, ppm): δ 163.1, 129.1, 127.0, 126.2, 111.7, 82.5.

2.4.2. Knoevenagel catalysis condensation reactions

All ILs were dried *in vacuo* at 60 °C for 4 h prior to use. ILs (2.0 mL, φ$_{IL}$ = 0.99) were heated in a Schlenk flask to 95 °C (internal temperature) prior to the addition of benzaldehyde (1.5 × 10^{-4} mol, 15 μL) and malononitrile (1.5 × 10^{-4} mol, 8 μL), with an internal standard of *p*-cymene (5 μL). All sample volumes were maintained at a total volume of 2.028 mL. The sample was then extracted with methanol (5 mL) and passed through a silica column before analysis on a Shimadzu GC-2010 Plus, fitted with a Restek Rtx-5MS column (30 mm × 0.25 mm, I.D.; 0.25 μm thickness) and a Shimadzu AOC-20i auto injector, a split ratio of 10 was used, with a 2.0 mL min^{-1} flow rate. Analysis was performed on Real Time analysis software. The conversions of substrate were determined by comparisons with a calibration curve established with 2-benzylidenemalononitrile (synthesis outlined in Section 2.4.1.).

3. Results and discussion

3.1. Structural characterization of bromozincate ILs

Single crystal X-ray diffraction analysis of the while solid precipitate of $[C_2Py]Br/ZnBr_2$ revealed an asymmetric unit cell composed of a tetrabromozincate dianion and two ethylpyridinium cations, of formula $[C_2Py]_2[ZnBr_4]$ (Fig. 2 (a), refer to ESI for crystallographic details).

Bromozincate anions of types $[ZnBr_4]^{2-}$ [25,26], $[Zn_2Br_6]^{2-}$ [14,27,28], and $[Zn_2Br_7]^{3-}$ [14] have been structurally characterised. However the structural characterisation of $[C_2Py]_2[ZnBr_4]$ is yet to be reported. Similar to previous characterisations, the dianion was shown to have a central zinc atom in a tetrahedral environment, with an average Br–Zn–Br angle of 109.4°, and average Zn—Br bond length of 2.417(3) Å. Each anion is surrounded by 8 cations, through the formation of 14 Br···H bonds. The average Br···H contact distance is 3.02(1) Å, less than the sum of the van der Waals radius (3.05 Å), indicating close interactions between the anion and cation. The Br···H interactions are not uniformly distributed for each bromide atom with the number of contacts varying between 2 and 5 contact points, indicating that several anion–cation interactions are stabilizing the structure.

An extended crystal structure viewed along the *b* axis, is shown in Fig. 2(b). The 3D network appears to be composed of two separate cation environments. One cation environment is composed of sheets orientated parallel to the *ab* plane, and are stabilized by close intermolecular quadrupole interactions between neighbouring pyridinium rings, with an average contact distance of 3.603(2) Å. The other cation environment forms planar sheets orientated parallel to the *ac* plane, and is stabilized by anion interactions, with no cation–cation interactions being present.

3.1.1. Lewis acidity of bromozincate ionic liquids

Lewis acidities of the ILs were studied to establish the relationship between activity and acidity. Using pyridine as a spectroscopic probe, the determination of Lewis acidity was achieved through examination of variations in the frequencies of the ring vibration absorptions [24]. Although this is technique does not measure the lewis acidity of the bulk IL, it can be used as a means determine relative Lewis acidities of the ILs used in this work.

As shown in Fig. 3, neat pyridine shows a resolved single absorption at 1437 cm^{-1}, resulting from the in-plane vibration of symmetry class B$_1$ [29]. With the addition of a Lewis acid shifts in absorption maxima are observed, due to the coordination of Lewis acidic sites with pyridine. Greater shifts in absorption maxima correspond to stronger Lewis acids.

As some ILs are solid at room temperature only a selected range of ILs were analysed for Lewis acidity. Consequently, a representative sample set, including $[C_6MIM]Br/ZnBr_2$, $[C_6M_2IM]Br/ZnBr_2$ and $[C_6Py]Br/ZnBr_2$ was used (Fig. 3). Fig. 3 (c), shows that a pyridine
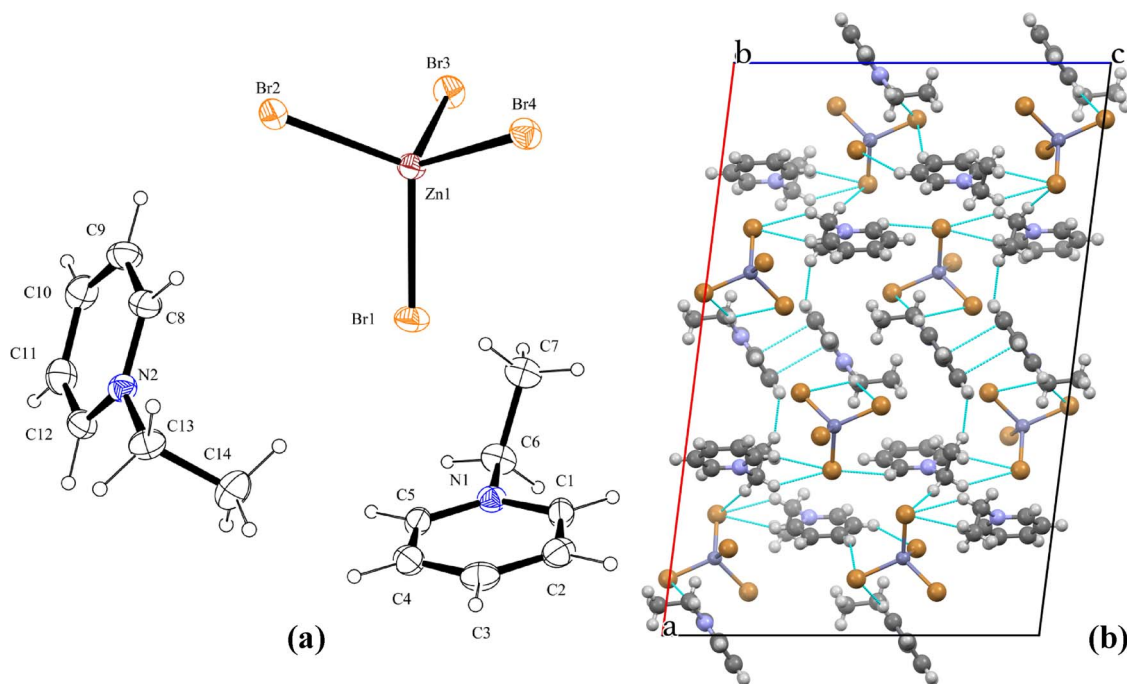
Fig. 2. (a) ORTEP depiction of single crystal X-ray crystallography results for *N*-ethylpyridinium tetrabromozincate, [C₂Py]₂[ZnBr₄] illustrating the 50% displacement ellipsoids with atomic labelling, (b) the extended lattice viewed along the *b* axis, to visualize cation interactions. Plotted in MERCURY, with orange spheres indicating the position of bromine atoms, dark purple spheres those of zinc atoms, light purple spheres illustrating nitrogen atoms, dark grey spheres illustrating carbon atoms and light grey spheres illustrating hydrogen atoms. See ESI for further information. (For interpretation of the references to colour in this figure legend, the reader is referred to the web version of this article.)
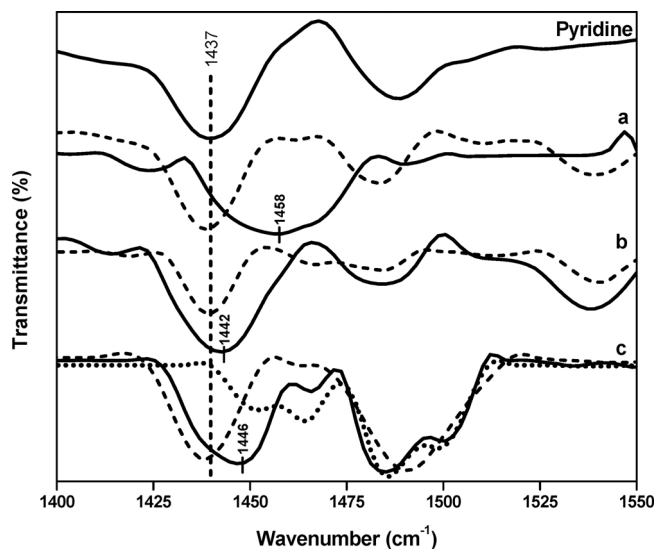

Fig. 3. FT-IR spectra for Lewis acidity determination of solutions composed of IL: pyridine (1:3 mass); (a) dashed: [C₆MIM][NTf₂], solid: [C₆MIM]Br/ZnBr₂; (b) dashed: [C₆M₂IM][NTf₂], solid: [C₆M₂IM]Br/ZnBr₂ (c) dashed: [C₆Py][NTf₂], solid: [C₆Py]Br/ZnBr₂, dotted: bulk [C₆Py]Br/ZnBr₂ (no pyridine added).

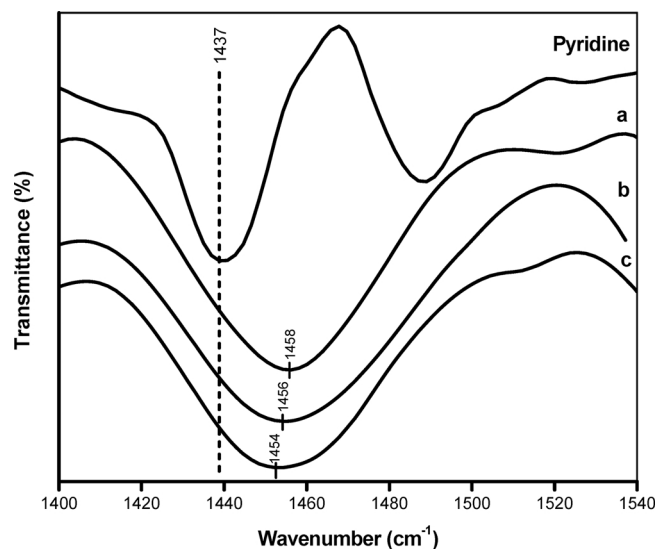**Fig. 4.** FT-IR spectra for Lewis acidity determination of solutions composed of IL: pyridine (1:3 mass); (a) [C₆MIM]Br/ZnBr₂; (b) [C₈MIM]Br/ZnBr₂; (c) [C₁₀MIM]Br/ZnBr₂.

between cation type and Lewis acid strength are consistent with the trends reported from other analytical techniques [30].

3.1.2. Cation alkyl chain length impact on Lewis acidity

Elongation of the alkyl chain length is expected to vary the Lewis acidity to a small extent. As the alkyl chain is shortened, stronger anion-cation interactions dominate, resulting in stronger Lewis acids [31]. This was probed spectroscopically as outlined in Section 3.1.1., with [C₆MIM]⁺, [C₈MIM]⁺ and [C₁₀MIM]⁺ bromozincate ILs analysed (Fig. 4). Only small variations in the absorption positions are seen with variation in the chain length, indicating that the anion is the major component determining Lewis acidity. [C₆MIM]Br/ZnBr₂ was shown to be the strongest Lewis acid (1458 cm⁻¹), followed by [C₈MIM]Br/

probe can be used to analyse pyridinium cations, without interference by the pyridinium ring vibrations.

For a simplistic comparison the analogous bis(trifluoromethane) sulfonimide ([NTf₂]⁺) ILs were mixed with pyridine (Fig. 3, dashed lines). It is evident that no absorption shift occurs with the [NTf₂]⁺ ILs, consistent with the lack of Lewis acidic sites. However, upon addition of the bromozincate ILs, the pyridine absorption shifts to 1458 cm⁻¹ for [C₆MIM]Br/ZnBr₂, 1446 cm⁻¹ for [C₆Py]Br/ZnBr₂ and 1442 cm⁻¹ for [C₆M₂IM]Br/ZnBr₂, indicating that the bromozincate ILs are Lewis acidic. These results demonstrate that the cation type does impact the Lewis acidity, with [C₆MIM]Br/ZnBr₂ being the strongest Lewis acid, and [C₆M₂IM]Br/ZnBr₂ being the weakest. The trends observed

Table 1
Summary of data derived from DFT modelling of the strength of non-covalent interactions between ions on the charge on the zinc atom.

Ionic Liquid	ΔG_{assoc} (kJ mol^{-1})	Charge on zinc
[C$_2$MIM]Br/ZnBr$_2$	−14.89	0.75918
[C$_4$MIM]Br/ZnBr$_2$	−19.30	0.75634

ZnBr$_2$ (1456 cm^{-1}) and [C$_{10}$MIM]Br/ZnBr$_2$ (1454 cm^{-1}) being the weakest Lewis acid.

To compliment this, standard density functional theory (DFT) calculations were used to model the influence of the alkyl chain elongation on Lewis acidity, and the charge on the zinc atom. Gaussian 09 [20] geometries and energies were obtained at the M05-2X/6-31G (d) level, combined with the SMD continuum solvation model [21,22]. The vibrational frequencies of the stationary points corresponded to the minima on the potential energy surface. Incorporated into the total energies are zero-point vibrational energies and thermal corrections for enthalpy and entropy derived from scaled M05-2X-D3/6- 31G(d) frequencies [23]. All free energies (kJ mol^{-1}) are reported as solvation-corrected at 298 K, and charges on zinc (Table 1) were calculated using natural bond orbital (NBO) analysis.

Elongation of the alkyl chain length from C$_2$ to C$_4$ (Fig. 5, Table 1) results in a slight decrease in the charge on the zinc atom, in-line with the trends observed spectroscopically. As the number of cation-bromine interactions increases, with increasing alkyl chain length, greater electron density is withdrawn from the zinc atom, resulting in a less positive charge and overall decreasing the Lewis acidity of the IL. Although the DFT studies provided show ion pair modelling which is likely to vary in a continuum solvent model used in this work, they are sufficient for clarification of the Lewis acidity trends observed from spectroscopic analysis.

3.1.3. Anion composition

As discussed in Section 3.1, [ZnBr$_4$]$^{2-}$ was isolated as the monomeric anion in the solid phase. However, it is likely that the bromozincate anion composition is polynuclear similar to the anions of chloroaluminate ILs. Probing the polymeric anion species was completed through Raman spectroscopy. Previously determined zinc bromide Raman absorptions are: 208 cm^{-1} for the bent ZnBr$_2$ moiety, 184 cm^{-1} for pyramidal [ZnBr$_3$]$^{-}$ and 172 cm^{-1} for the [ZnBr$_4$]$^{2-}$ tetrahedral arrangement [32]. Fig. 6, shows the Raman spectra of neat [C$_4$MIM]Br/ZnBr$_2$, [C$_4$M$_2$IM]Br/ZnBr$_2$ and [C$_4$Py]Br/ZnBr$_2$. It is clear that the IL bromozincate anions are, in fact, a series of polyanions, with both [C$_4$MIM]Br/ZnBr$_2$ and [C$_4$Py]Br/ZnBr$_2$ containing [ZnBr$_4$]$^{2-}$ and [ZnBr$_3$]$^{-}$ anions. None of the spectra of the ILs examined showed the presence of ZnBr$_2$, demonstrating the tendency for formation of higher order bromozincate anionic species. Of note is the anion composition of [C$_4$M$_2$IM]Br/ZnBr$_2$ the Raman spectrum of which indicated only [ZnBr$_4$]$^{2-}$, as shown in Fig. 6. This may be due to the large number of
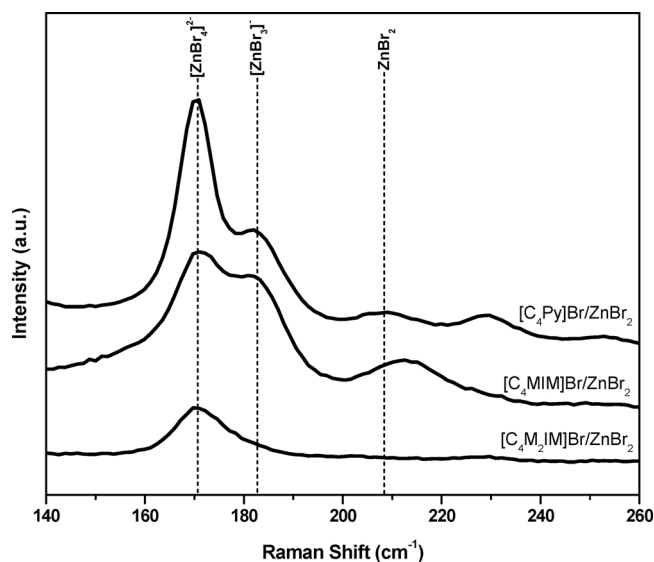
Fig. 6. Neat Raman spectra of selected bromozincate ILs, absorptions of ZnBr$_2$ at 208 cm^{-1}, [ZnBr$_3$]$^{-}$ at 184 cm^{-1} and [ZnBr$_4$]$^{2-}$ at 172 cm^{-1}.

Br···H interactions stabilizing the dianion, similar to that observed in the crystallographic study (section 3.1).

3.2. Bromozincate ILs in the Knoevenagel condensation reaction

The condensation between benzaldehyde and malononitrile was studied in a range of [C$_n$MIM]Br/ZnBr$_2$, [C$_n$M$_2$IM]Br/ZnBr$_2$ and [C$_n$Py]Br/ZnBr$_2$ (n = 2, 4, 6, 8, 10) ILs to explore the effect of both Lewis acidity and domain heterogeneity. Based on log(P$_{ow}$) values benzaldehyde is predicted to solvate into the non-polar domain, while malononitrile was likely to solvate into both domains likely solvating at the interface of the two domains (Table 2).

It is noteworthy that the volume fraction of IL employed for all reactions was maintained at 0.99 to ensure that the IL was the bulk of the reaction medium. Hence, elongation of the alkyl chain will correspond to a greater non-polar domain, and a corresponding decrease in the polar domain. The anion was assumed to be [ZnBr$_3$]$^{-}$ to allow for the calculation of domain sizes. Further information and calculations of the polar (V$_p$) and non-polar domain (V$_{np}$) volumes are detailed in the ESI. All reactions were 100% selective for the product (sample chromatogram is in ESI).

Reactions in ILs with smaller non-polar domain volumes were predicted to have higher conversion, this was observed for both the [C$_n$MIM]Br/ZnBr$_2$ and the [C$_n$Py]Br/ZnBr$_2$ series. However, the [C$_n$M$_2$IM]Br/ZnBr$_2$ series showed that a reaction in [C$_4$M$_2$IM]Br/ZnBr$_2$ (88.4%) had higher conversion than one in [C$_2$M$_2$IM]Br/ZnBr$_2$
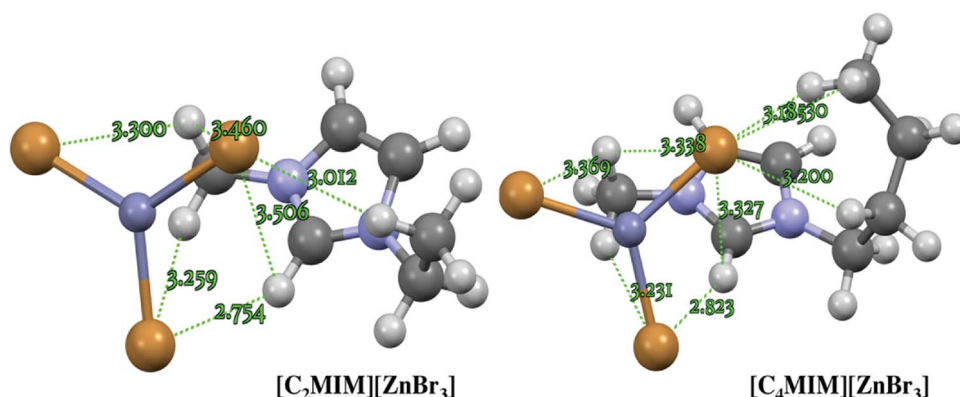
Fig. 5. DFT energy-minimized structures for [C$_n$MIM]Br/ZnBr$_2$ ILs (n = 2, 4) plotted in MERCURY. Short-range contact distances between the anion–cation are shown.

[C$_2$MIM][ZnBr$_3$]

[C$_4$MIM][ZnBr$_3$]

Table 2

Product conversion for the Knoevenagel condensation reaction between benzaldehyde and malononitrile. Uncertainty is calculated as the standard deviation of three repeat experiments.

Ionic liquid	V_{np} (mL)	V_p (mL)	% Conversion to product
$[C_2MIM]Br/ZnBr_2$	0.242	1.786	86.2 ± 0.9
$[C_4MIM]Br/ZnBr_2$	0.470	1.558	78.5 ± 1.2
$[C_6MIM]Br/ZnBr_2$	0.665	1.363	69.6 ± 0.7
$[C_8MIM]Br/ZnBr_2$	0.807	1.221	56.9 ± 1.4
$[C_{10}MIM]Br/ZnBr_2$	0.921	1.107	37.3 ± 2.0
$[C_2M_2IM]Br/ZnBr_2$	0.224	1.804	82.7 ± 1.0
$[C_4M_2IM]Br/ZnBr_2$	0.452	1.576	88.4 ± 1.5
$[C_6M_2IM]Br/ZnBr_2$	0.626	1.402	52.5 ± 1.6
$[C_8M_2IM]Br/ZnBr_2$	0.765	1.263	40.1 ± 2.1
$[C_{10}M_2IM]Br/ZnBr_2$	0.877	1.151	29.3 ± 1.9
$[C_2Py]Br/ZnBr_2$	0.247	1.781	84.2 ± 1.6
$[C_4Py]Br/ZnBr_2$	0.493	1.535	69.5 ± 1.3
$[C_6Py]Br/ZnBr_2$	0.676	1.352	60.8 ± 0.7
$[C_8Py]Br/ZnBr_2$	0.819	1.209	45.3 ± 0.8
$[C_{10}Py]Br/ZnBr_2$	0.934	1.094	32.0 ± 1.2

Table 3

Adjustment of anion composition and recalculation of domain sizes.

Ionic Liquid	V_{np} (mL)	V_p (mL)	% Conversion to product
$[C_4M_2IM][ZnBr_3]$	0.452	1.576	–
$[C_4M_2IM]_2[ZnBr_4]$	0.213	1.815	88.4 ± 1.5
$[C_2M_2IM][ZnBr_3]$	0.224	1.804	82.7 ± 1.0

4. Conclusions

This work demonstrates the synthesis of a range of bromozincate based ILs, with the anion composition and Lewis acidity determined spectroscopically. Additionally, the crystal structure of $[C_2Py]_2[ZnBr_4]$ is reported. The bromozincate ILs were used as both Lewis acid catalysts and solvents in the Knoevenagel condensation reaction, as a test reaction. It was demonstrated that numerous factors influence reaction outcomes including domain size, Lewis acidity as well as anion composition. These conclusions provide an insight into the complexity of ILs and how the systems can be manipulated to achieve specific reaction outcomes.

Appendix A. Supplementary data

Supplementary data associated with this article can be found, in the online version, at http://dx.doi.org/10.1016/j.apcatb.2017.09.021.
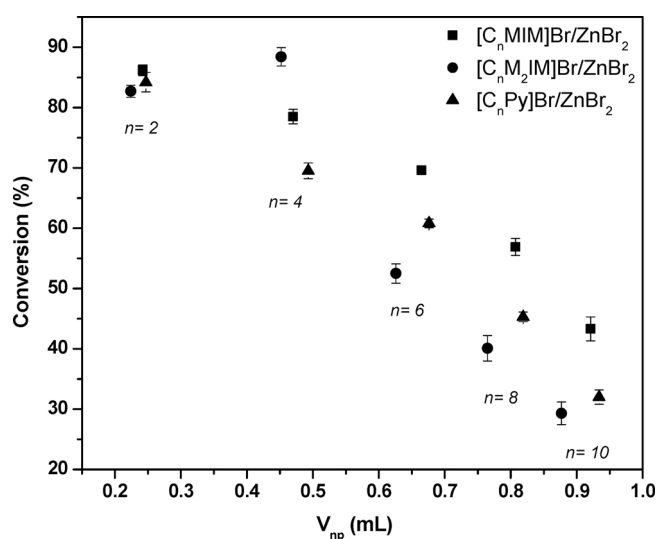

Fig. 7. Substrate conversion (%) with respect to the volume of the non-polar domain (V_{np}). Calculations and exact V_{np} is outlined in the ESI.

(82.7%), contrary to expected results.

The Lewis acid strength of the ILs (determined in Section 3.1.1) was also expected to impact conversions. In analogous series, the strongest Lewis acidic ILs, $[C_nMIM]Br/ZnBr_2$ showed highest conversions, followed by those in $[C_nPy]Br/ZnBr_2$ and those reactions in the weakest Lewis acids, $[C_nM_2IM]Br/ZnBr_2$ had lowest conversion (Fig. 7). This is consistent for all tested ILs, with the exception of $[C_4M_2IM]Br/ZnBr_2$. The reaction in $[C_4M_2IM]Br/ZnBr_2$ (88.4%) showed higher conversion than those in either $[C_4Py]Br/ZnBr_2$ (69.5%) or $[C_4MIM]Br/ZnBr_2$ (78.5%) despite $[C_4M_2IM]Br/ZnBr_2$ being a weaker Lewis acid.

The Raman spectra of $[C_4M_2IM]Br/ZnBr_2$ (Section 3.1.3) showed the presence of only the $[ZnBr_4]^{2-}$ dianion. Hence, the assumption of $[ZnBr_3]^-$ as the IL anion used for domain volume calculations was not appropriate for this particular IL. The results of recalculation of the domain size assuming the formula $[C_4M_2IM]_2[ZnBr_4]$ are shown in Table 3. For $[C_4M_2IM]_2[ZnBr_4]$ the V_{np} is calculated to be 0.213 mL, significantly less than that calculated for the formulation $[C_4M_2IM][ZnBr_3]$. Comparison of the conversion of the reaction in an IL with composition $[C_4M_2IM]_2[ZnBr_4]$ (88.4%), with one of composition $[C_2M_2IM][ZnBr_3]$ (82.7%), shows that based on the smaller V_{np} of the composition $[C_4M_2IM]_2[ZnBr_4]$ it can be concluded that the higher conversion is a result of the domain nanostructure.

References

[1] B.C. Ranu, S. Banerjee, Tetrahedron Lett. 48 (2007) 141–143.
[2] C. Yue, M. Aiqin, Yunyang Wei, Lu Minjie, Cat. Commun. 9 (2008) 1571–1574.
[3] G. Zhao, T. Jiang, H. Gao, B. Han, J. Huang, D. Sun, Green Chem. 6 (2004) 75–77.
[4] T. Jiang, H. Gao, B. Han, G. Zhao, Y. Chang, W. Wu, L. Gao, G. Yang, Tetrahedron Lett. 45 (2004) 2699–2701.
[5] K.F. Shelke, B.R. Madje, S.B. Sapkal, B.B. Shingate, M.S. Shingare, Green Chem. Lett. 2 (2009) 3–7.
[6] Y. Wang, G.A. Voth, J. Phys. Chem. 110 (2006) 18601–18608.
[7] C.C. Weber, A.F. Masters, T. Maschmeyer, Green Chem. 15 (2013) 2655–2679.
[8] J.N.A. Canongia Lopes, A.A.H. Pádua, J. Phys. Chem. B 110 (2006) 3330–3335.
[9] J. Wishart, J. Phys. Chem. Lett. 1 (2010) 1629–1630.
[10] C.C. Weber, A.F. Masters, T. Maschmeyer, Org. Biomol. Chem. 11 (2013) 2534–2542.
[11] A.R. Hajipour, F. Rafiee, J. Iranian, Chem. Soc. 6 (2009) 647–678.
[12] A.M. Paul, A.C. Khandekar, B.M. Khadilkar, J. Chem. Res. (2003) 168–169.
[13] B. Gilbert, H. Olivier-Bourbigou, F. Favre, Oil Gas Sci. Technol. Rev. IFP 62 (2007) 745–759.
[14] M.E. Easton, P. Turner, A.F. Masters, T. Maschmeyer, RSC Adv. 5 (2015) 83674–83681.
[15] A.B. Pangborn, M.A. Giardello, R.H. Grubbs, R.K. Rosen, F.J. Timmers, Organomet 15 (1996) 1518–1520.
[16] A.K. Burrell, R.E.D. Sesto, S.N. Baker, T.M. McCleskey, G.A. Baker, Green Chem. 9 (2007) 449–454.
[17] A.P. Abbott, G. Capper, D.L. Davies, H.L. Munro, R.K. Rasheed, V. Tambyrajah, Chem. Commun. 201 (2001) 0–201 (1).
[18] G.M. SHELX, Sheldrick, University of Göttingen, Germany (2014).
[19] G.M. Sheldrick, Acta Crystallogr. A 64 (2008) 112–122.
[20] M.J. Frisch, G.W. Trucks, H.B. Schlegel, G.E. Scuseria, M.A. Robb, J.R. Cheeseman, G. Scalmani, V. Barone, B. Mennucci, G.A. Petersson, H. Nakatsuji, M. Caricato, X. Li, H.P. Hratchian, A.F. Izmaylov, J. Bloino, G. Zheng, J.L. Sonnenberg, M. Hada, M. Ehara, K. Toyota, R. Fukuda, J. Hasegawa, M. Ishida, T. Nakajima, Y. Honda, O. Kitao, H. Nakai, T. Vreven, J.A. Montgomery Jr., J.E. Peralta, F. Ogliaro, M.J. Bearpark, J. Heyd, E.N. Brothers, K.N. Kudin, V.N. Staroverov, R. Kobayashi, J. Normand, K. Raghavachari, A.P. Rendell, J.C. Burant, S.S. Iyengar, J. Tomasi, M. Cossi, N. Rega, N.J. Millam, M. Klene, J.E. Knox, J.B. Cross, V. Bakken, C. Adamo, J. Jaramillo, R. Gomperts, R.E. Stratmann, O. Yazyev, A.J. Austin, R. Cammi, C. Pomelli, J.W. Ochterski, R.L. Martin, K. Morokuma, V.G. Zakrzewski, G.A. Voth, P. Salvador, J.J. Dannenberg, S. Dapprich, A.D. Daniels, Ö. Farkas, J.B. Foresman, J.V. Ortiz, J. Cioslowski, D.J. Fox, Gaussian 09, Gaussian, Inc, Wallingford, CT, USA, 2009.
[21] A.V. Marenich, C.J. Cramer, D.G. Truhlar, J. Phys. Chem. B 113 (2009) 6378–6396.

[22] Y. Zhao, N.E. Schultz, D.G. Truhlar, J. Chem, Theory Comput. 2 (2006) 364–382.
[23] J.P. Merrick, D. Moran, L. Radom, J. Phys. Chem. A 111 (2007) 11683–11700.
[24] Y.-l. Yang, Y. Kou, Chem. Commun. (2004) 226–227.
[25] B.F. Ali, S.F. Haddad, R. Al-Far, Acta Crystallogr. E 68 (2012) m1320.
[26] B.F. Ali, R. Al-Far, Acta Crystallogr. E 65 (2009) m581–m582.
[27] R. Duhlev, R. Faggiani, I.D. Brown, Acta Crystallogr. C 43 (1987) 2046–2048.
[28] R. Duhlev, I.D. Brown, R. Faggiani, Acta Crystallogr. C 44 (1988) 1696–1698.
[29] J. Serratosa, Infrared analysis of the orientation of pyridine molecules in clay

complexes, Clays and Clay Minerals: Proceedings of the Fourteenth National Conference, Berkeley, California, Elsevier, 2013 (p. 385).
[30] M.A. Ab Rani, A. Brant, L. Crowhurst, A. Dolan, M. Lui, N.H. Hassan, J.P. Hallett, P.A. Hunt, H. Niedermeyer, J.M. Perez-Arlandis, M. Schrems, T. Welton, R. Wilding, Phys. Chem. Chem. Phys. 13 (2011) 16831–16840.
[31] A. Aggarwal, N.L. Lancaster, A.R. Sethi, T. Welton, Green Chem. 4 (2002) 517–520.
[32] M. Yang, D. Crerar, D. Irish, J. Solution Chem. 17 (1988) 751–762.